JGR Space Physics

RESEARCH ARTICLE
10.1029/2020JA028360

Ionospheric Signatures of Secondary Waves From Quasi-6-Day Wave and Tide Interactions

Y. Yamazaki[1] and **Y. Miyoshi**[2]

[1]GFZ German Research Centre for Geosciences, Potsdam, Germany, [2]Department of Earth and Planetary Sciences, Kyushu University, Fukuoka, Japan

This article is a companion to Miyoshi and Yamazaki (2020), https://doi.org/10.1029/2020JA028283.

Key Points:

- Spectrum analysis is performed on total electron content during the quasi-6-day wave event in September 2019
- Signatures of secondary waves from the non-linear interaction of the quasi-6-day wave with tides are detected
- The wave signatures result from the modulation of the equatorial plasma fountain

Correspondence to:
Y. Yamazaki,
yamazaki@gfz-potsdam.de

Citation:
Yamazaki, Y., & Miyoshi, Y. (2021). Ionospheric signatures of secondary waves from quasi-6-day wave and tide interactions. *Journal of Geophysical Research: Space Physics*, *126*, e2020JA028360. https://doi.org/10.1029/2020JA028360

Received 15 JUN 2020
Accepted 6 MAR 2021

Abstract A sudden stratospheric waring occurred in the southern hemisphere during September 2019, accompanied by an exceptionally strong quasi-6-day wave (Q6DW). We examine the ionospheric response using global total electron content (TEC) maps, with a focus on the short-period variability (5–48 h). A Fourier analysis of the TEC data reveals ionospheric variations associated with the secondary waves due to the non-linear interaction between the Q6DW and atmospheric tides. The largest signatures among them are related to the ~29-h standing oscillation, which is attributable to the Q6DW interaction with the migrating diurnal tide, with the maximum amplitude ~8% of the zonal mean. Also detected are the signatures associated with the westward-propagating ~13-h oscillation with the zonal wavenumber 1 (~4%) and westward-propagating ~11-h oscillation with the zonal wavenumber 3 (~3%), both of which can be attributed to the Q6DW interaction with the migrating semidiurnal tide. The signatures related to the Q6DW interaction with the migrating terdiurnal tide and some non-migrating tides are also observed. This is the first time that secondary wave signatures of the Q6DW-tidal interaction are identified in ionospheric observations with predicted zonal wavenumbers and periods. The oscillations are symmetric about the magnetic equator with amplitude peaks at ±20° magnetic latitudes, suggesting that the oscillations are generated by the modulation of the equatorial plasma fountain.

1. Introduction

The state of the ionosphere significantly changes from day to day. The ionospheric weather is controlled not only by forcing from above (e.g., solar radiation and energy deposition from the magnetosphere) but also by forcing from below, through upward-propagating waves, such as planetary waves, tides, and gravity waves (e.g., Liu, 2016). Sudden stratospheric warmings (SSWs) are extreme meteorological events that disturb the whole atmosphere (e.g., Chau et al., 2012; Pedatella et al., 2018) and thus provide opportunities to study vertical atmospheric coupling processes including their influences on the ionosphere. Most previous studies on the ionospheric response to SSWs focused on northern hemisphere events (e.g., Goncharenko et al., 2010, 2013; Oberheide et al., 2020). In the southern hemisphere, SSWs are not as frequent or as intense because of weaker wave forcing from the troposphere as the result of smaller topographical differences and land-sea contrasts. The September 2002 SSW was the only "major" warming event recorded in the southern hemisphere, according to the SSW classification developed for northern hemisphere events (Krüger et al., 2005). Identifying ionospheric effects of the September 2002 SSW was, however, difficult because of geomagnetic storms that took place around the same time (Olson et al., 2013).

As recently reported by Yamazaki, Matthias, et al. (2020, hereafter Y20), there was an Antarctic SSW in September 2019 under relatively quiet geomagnetic activity conditions. Although the September 2019 SSW was a "minor" warming without the polar vortex breakdown at 10 hPa (~32 km altitude), it involved an unprecedentedly large increase in the stratospheric polar temperature by more than 50 K per week, which is comparable with major SSWs in the northern hemisphere. Using geopotential height (GPH) data from the Aura satellite, Y20 showed that during the SSW, the quasi-6-day wave (Q6DW) was unusually strong in the mesosphere and lower thermosphere (MLT) region, with the amplitude being approximately four times as large as the seasonal climatological value. The Q6DW is a westward-propagating planetary wave with zonal wavenumber one and period around 6 days, which is occasionally observed in the middle atmosphere (e.g., Forbes & Zhang, 2017; Riggin et al., 2006). Y20 also showed ionospheric variations with a period of ~6 days in low-latitude electric currents and plasma densities at the time of enhanced Q6DW activity during the

September 2019 SSW using Swarm satellite measurements. Lin et al. (2020) examined global characteristics of these 6-day variations using an ionospheric data assimilation product.

The main objective of this study is to present observations of short-period variability (5–48 h) in the ionosphere during the September 2019 SSW and discuss the source of the variability. In the accompanying paper, Miyoshi and Yamazaki (2020) (hereafter MY20), we presented whole-atmosphere simulations of the September 2019 SSW by the Ground-to-topside model of Atmosphere and Ionosphere for Aeronomy (GAIA). The simulation results suggested that secondary waves arising from the non-linear interaction between the Q6DW and tides played a significant role in driving 6-day variations in the ionosphere during the SSW. This was supported by Swarm observations of Y20, which detected 6-day variations in ionospheric data collected in the noon local time sector. However, these secondary waves have periods close to tides (24 h, 12 h, 8 h, ...) and could not be fully resolved in the Swarm data due to the limited spatial and temporal coverage of the satellite. In this study, we use global TEC maps to gain a more complete picture of ionospheric variability during the September 2019 SSW.

Before preceding further, we define the nomenclature of atmospheric waves that is used throughout the remainder of this paper. In general, a wave in an atmospheric parameter can be expressed in the form:

$$A\cos\left(n\Omega t + s\lambda - \phi\right) \tag{1}$$

where t is the universal time in days, λ is the longitude in radians, Ω is the Earth's rotation rate ($=2\pi$/day), and n (≥ 0) is the frequency (/day). s ($= \ldots -3, -2, -1, 0, +1, +2, +3, \ldots$) is the zonal wavenumber, A is the amplitude and ϕ is the phase. Waves with $s > 0$ and $s < 0$ propagate westward and eastward, respectively, and waves with $s = 0$ represent standing oscillations.

Atmospheric tides (Lindzen & Chapman, 1969) have a frequency of the Earth's rotation ($n = 1$) or its harmonics ($n = 2, 3, 4, \ldots$). Tides with $n = 1$, 2, and 3 are referred to as diurnal, semidiurnal, and terdiurnal tides. Tides that satisfy $n = s$ are called "migrating" tides. They have the zonal phase speed $\frac{D\lambda}{Dt} = -\Omega$, thus propagate westward with the same speed as the apparent motion of the Sun; in other words, migrating tides are sun-synchronous. All other non-sun-synchronous tides ($n \neq s$) are called "non-migrating" tides. Following earlier work (e.g., Forbes et al., 2008), we use the notion DW*s*, SW*s*, and TW*s* to denote westward propagating diurnal, semidiurnal, and terdiurnal tides, respectively, with the zonal wavenumber *s*. For eastward propagating tides, "E" replaces "W." Standing oscillations ($s = 0$) are denoted as D0, S0, and T0, respectively.

According to the theory of Teitelbaum and Vial (1991), the non-linear interaction of two global-scale waves generate secondary waves with frequencies and zonal wavenumbers that are the sums and differences of those of the interacting waves. For instance, the non-linear interaction of the Q6DW ($n = n_6, s = +1$) and migrating diurnal tide DW1 ($n = 1, s = +1$) can lead to the secondary waves ($n = 1 - n_6, s = 0$) and ($n = 1 + n_6, s = +2$), which have periods of ~29 and ~21 h, and thus are referred to as 29h0 and 21hW2, respectively. By the same token, the non-linear interaction between the Q6DW and migrating semidiurnal tide SW2 ($n = 2, s = +2$) can generate the secondary waves 13hW1 ($n = 2 - n_6, s = +1$) and 11hW3 ($n = 2 + n_6, s = +3$), and the non-linear interaction between the Q6DW and migrating terdiurnal tide TW3 ($n = 3, s = +3$) can cause the secondary waves 8.5hW2 ($n = 3 - n_6, s = +2$) and 7.5hW4 ($n = 3 + n_6, s = +4$). Secondary waves can also be generated by the non-linear interaction of the Q6DW and non-migrating tides. For example, the Q6DW interaction with DE3 ($n = 1, s = -1$) can generate the secondary waves 29hE4 ($n = 1 - n_6, s = -4$) and 21hE2 ($n = 1 + n_6, s = -2$).

Radar observations of mesospheric winds have provided evidence to support the presence of the secondary waves associated with the non-linear interaction between the Q6DW and tides (e.g., Beard et al., 1999; Pancheva et al., 2003). The wave signatures can be detected as they appear as "sidebands" of tides in the periodogram. However, it is often difficult to uniquely determine the zonal wavenumber of the secondary waves due to limited longitudinal coverage. Satellite observations also have difficulties in resolving the secondary waves because of limited spatial and temporal coverage. Forbes and Zhang (2017), using temperature data in the middle atmosphere from the Thermosphere Ionosphere Mesosphere Energetics and Dynamics (TIMED) satellite, observed variations that are attributable to secondary waves from the Q6DW-tidal interaction. However, it was difficult to uniquely identify the source wave because of the ambiguity caused

by aliasing. For instance, when observed from the TIMED satellite perspective, the secondary waves from the Q6DW and migrating tides such as 29h0 and 13hW1 have nearly the same frequency as the Q6DW, and thus they are indistinguishable.

Modeling studies have provided further evidence to support the non-linear interaction between the Q6DW and tides. Pedatella et al. (2012) presented idealized simulations by the thermosphere–ionosphere–mesosphere electrodynamics general circulation model (TIME-GCM). The analysis of the simulation results revealed the presence of 29h0 and 21hW2 due to the Q6DW–DW1 interaction, as well as 29hE4 and 21hE2 due to the Q6DW–DE3 interaction. Gan et al. (2017) also performed idealized TIME-GCM simulations and found 29h0, 21hW2, 13hW1, and 11hW3 in neutral winds. Some of these wave signatures also appeared in ionospheric parameters such as equatorial vertical plasma drift velocity and peak electron density N_mF_2. In MY20, we predicted the presence of 13hW1 and 11hW3 in neutral winds during the September 2019 SSW using the GAIA model.

As outlined above, secondary waves from the Q6DW-tidal interaction are still to be unambiguously identified in observational data, and their ionospheric effects need to be quantified. The strong Q6DW event in September 2019 provides an opportunity to investigate the ionospheric response to the secondary waves. The present study aims to (1) identify secondary wave signatures in the ionosphere with zonal wavenumbers and periods, (2) quantify the ionospheric variations associated with the secondary waves, and (3) evaluate the relative importance of different secondary waves, none of which has been achieved in previous observational studies. In addition, the GAIA model can shed light on the mechanism by which ionospheric signatures of the secondary waves are produced.

2. Data, Analysis Method, and Model

We use Universitat Politècnica de Catalunya (UPC) global ionospheric maps (GIMs) of vertical TEC derived with global positioning system (GPS) measurements from globally distributed ground stations (Hernández-Pajares et al., 2009). UPC GIMs (e.g., Orús et al., 2005; Roma-Dollase et al., 2018) have a spatial resolution of 2.5° in latitude and 5.0° in longitude, and a time resolution of 15 min. A coordinate transformation from geographic to Quasi-Dipole coordinates (Emmert et al., 2010) was conducted, and a Fourier analysis was performed on the TEC data at each magnetic latitude. A 21-day window was used in the Fourier analysis, which achieves a reasonable trade-off between the time and frequency resolutions. As will be shown later, this is approximately the duration of the Q6DW event in September 2019.

We also use simulation data from GAIA (e.g., Jin et al., 2011; Miyoshi et al., 2011). Briefly, GAIA is a numerical representation of the Earth's whole atmosphere from the surface to the upper thermosphere (up to $\sim 10^{-9}$ hPa). GAIA consists of the whole atmosphere GCM of Miyoshi and Fujiwara (2003), ionospheric model of Shinagawa (2011), and electrodynamics model of Jin et al. (2008), which are coupled to one another. The whole atmosphere GCM has the horizontal resolution of 2.8° in longitude and latitude and the vertical resolution of a grid per 0.2 scale height. The lower part of the GCM below 40 km was constrained with the meteorological reanalysis JRA-55 (Kobayashi et al., 2015) using a nudging technique similar to those used by Jin et al. (2012) and Miyoshi et al. (2017). This serves as forcing from the lower atmosphere to the upper layers, thus enabling GAIA to reproduce the ionospheric response to meteorological forcing from below (e.g., Pancheva et al., 2012; Yamazaki, Miyoshi, et al., 2020). Simulations were performed for solar minimum conditions that were held constant using a solar activity index $F_{10.7}$ value of 68 solar flux unit (SFU; 10^{-22} W m^{-2} Hz^{-1}). Geomagnetically quiet conditions were assumed by setting the cross polar cap potential to a low and constant value of 30 kV. Thus, ionospheric day-to-day variability in GAIA arises from meteorological forcing but not from solar radiation forcing or magnetospheric forcing. TEC was derived by vertically integrating the electron density from the ground to the top boundary of the ionospheric model, ~2,000 km. The simulation data are archived at GFZ Data Services (Yamazaki & Miyoshi, 2020).

MY20 presented GAIA simulations of the September 2019 Arctic SSW. It was demonstrated that GAIA is able to reproduce salient features of the middle atmosphere response to the SSW, including the zonal mean zonal wind and temperature, and enhanced Q6DW activity. GAIA is also able to reproduce the ionospheric response in the equatorial electrojet intensity and low-latitude TEC as observed by the Swarm satellite in the noon local-time sector. MY20 also presented simulations with modified wind forcing to the ionosphere.

We use one of those simulations, along with the original GAIA simulation. In the modified simulation, the whole atmosphere GCM of GAIA was reconstructed with large-scale waves with $|s| \leq 5$ and periods shorter than 36 h based on the spectral analysis technique of Hayashi (1971), and the reconstructed neutral atmosphere was used to force the ionospheric and electrodynamics models. Thus, the modified simulation excludes forcing to the ionosphere by the Q6DW and other long-period waves, while it retains forcing due to tidal modulation by the Q6DW.

Other data used in this study include the zonal wind and temperature from the meteorological reanalysis MERRA-2 (Gelaro et al., 2017) and the GPH measurements from the microwave limb sounder (MLS) onboard the Aura satellite (Schwartz et al., 2008; Waters et al., 2006), as well as the solar flux index $F_{10.7}$ (Tapping, 2013) and geomagnetic activity index Ap.

3. Results and Discussion

3.1. September 2019 SSW

Figure 1 gives an overview of the September 2019 Antarctic SSW event. Figure 1a shows the meridional temperature gradient over the southern hemisphere high-latitude region, as derived from the MERRA-2 reanalysis. The temperature gradient is defined here as the zonal-mean temperatures at 10 hPa (~32 km) averaged from 90° to 80°S minus the temperatures averaged from 70° to 60°S. According to the seasonal climatology, defined here as the mean values for 1980–2018 (black dashed line), the temperature gradient is usually negative throughout September, and it turns positive around 10 October, representing the seasonal transition. In 2019 (red line), the reversal of the temperature gradient took place much earlier on 6 September due to the SSW and it did not turn back negative for the rest of the period. The time evolution of the temperature gradient in 2019 deviates significantly from those in other years during 1980–2018 (gray lines).

Figure 1b presents the zonal mean zonal wind at 60°S and 1 hPa (~48 km). In the seasonal climatology (black dashed line), the zonal mean flow is eastward during the whole period from 15 August to 15 October. The 2019 data (red line) reveal a reduced eastward wind starting from 28 August. There is a westward turning of the zonal mean flow on 7 September, which lasted until 21 September. The maximum westward wind of −12.6 m/s was observed on 14 September. As noted by Y20, there was no wind reversal in the lower stratosphere, at 10 hPa (~32 km), and thus this SSW event is classified as a minor warming.

Enhanced Q6DW activity during the September 2019 SSW is depicted in Figure 1c. It shows the amplitude of the westward-propagating wave with zonal wavenumber 1 in Aura/MLS GPH at 0.001 hPa (~96 km) as a function of time and period (in days). Following Yamazaki (2018), the component of GPH perturbations that is symmetric about the equator was analyzed. Yamazaki (2018) demonstrated that the 6-day oscillation in the low-latitude ionosphere is enhanced when the symmetric component of the Q6DW is large in the lower thermosphere. In Figure 1c, strong Q6DW activity is seen throughout the second half of September 2019, with the maximum amplitude of 0.4 km observed on 20 September. This Q6DW event is strongest among those observed by the Aura/MLS since August 2004. All other Q6DW events in 2004–2019 have the maximum amplitude less than 0.3 km at the same latitude and height.

Daily values of $F_{10.7}$ and Ap indices are plotted in Figures 1d and 1e, respectively. It is well known that both solar (i.e., $F_{10.7}$) and geomagnetic (i.e., Ap) activity can influence the ionosphere. As seen in Figure 1d, solar activity stayed low with little variation throughout the investigated period. Geomagnetic activity (Figure 1e) was also low for most of the time, but it exhibits some variability with moderately enhanced activity on August 31 and 27 September. Figure 1f presents the wavelet spectrum of the Ap index. It is seen that the spectrum is dominated by the well-known periods of 27 and 13.5 days, which are associated with the solar rotation. The 6-day component is small during the Q6DW event in the second half of September 2019 (Figure 1c).

3.2. Short-Period Wave Signatures in TEC

Figure 2 displays Fourier spectra of TEC at 20°N (left column) and 20°S (right column) magnetic latitudes during 10–30 September 2019. Each row corresponds to the results with a different zonal wavenumber. In each panel, the red line shows the result for 2019, while the green shading indicates the maximum and

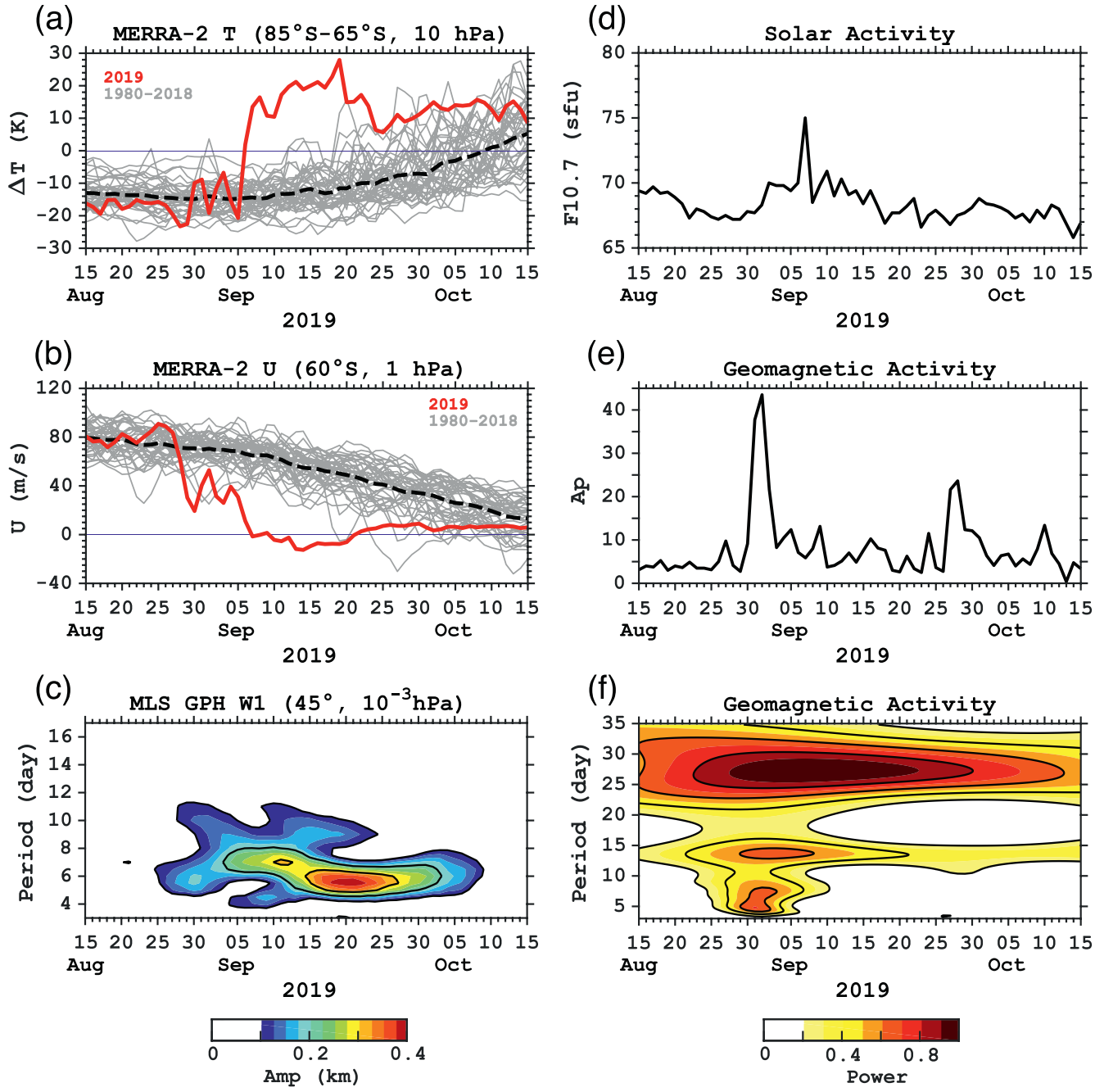

Figure 1. Overview of the middle atmosphere dynamics during the September 2019 Antarctic sudden stratospheric warming. (a) The meridional gradient of the zonal-mean temperature poleward of 60°S latitude at 10 hPa (~32 km altitude) derived from the MERRA-2 reanalysis. The red line shows the daily values for 2019, while the gray lines show the data for 1980 to 2018. The black dashed line shows the climatological mean values for 1980 to 2018. (b) The zonal mean zonal wind at 60°S latitude at 1 hPa (~48 km altitude) derived from the MERRA-2 reanalysis. The red line is for 2019, while the gray lines are for 1980 to 2018. The black dashed line represents the climatological seasonal cycle. (c) The amplitude of the westward-propagating wave with zonal wavenumber 1 in the equatorially symmetric component of geopotential height perturbations at 45° latitude and 0.001 hPa (~96 km altitude) observed by the Aura MLS. (d) Daily values of the solar activity index $F_{10.7}$. (e) Daily values of the geomagnetic activity index *Ap*. (f) Wavelet spectrum of the geomagnetic activity index *Ap*. The color indicates the normalized power. MLS, microwave limb sounder.

minimum values obtained during the same time of other years (2011–2018 and 2020), and the gray line is the average of the results for those years. The horizontal axis represents the frequency (/day) of wave components and the vertical axis represents the logarithm of the amplitude (in %) of the waves relative to the zonal mean TEC. Despite changes in solar activity over the years, it is possible to compare the 2019 results

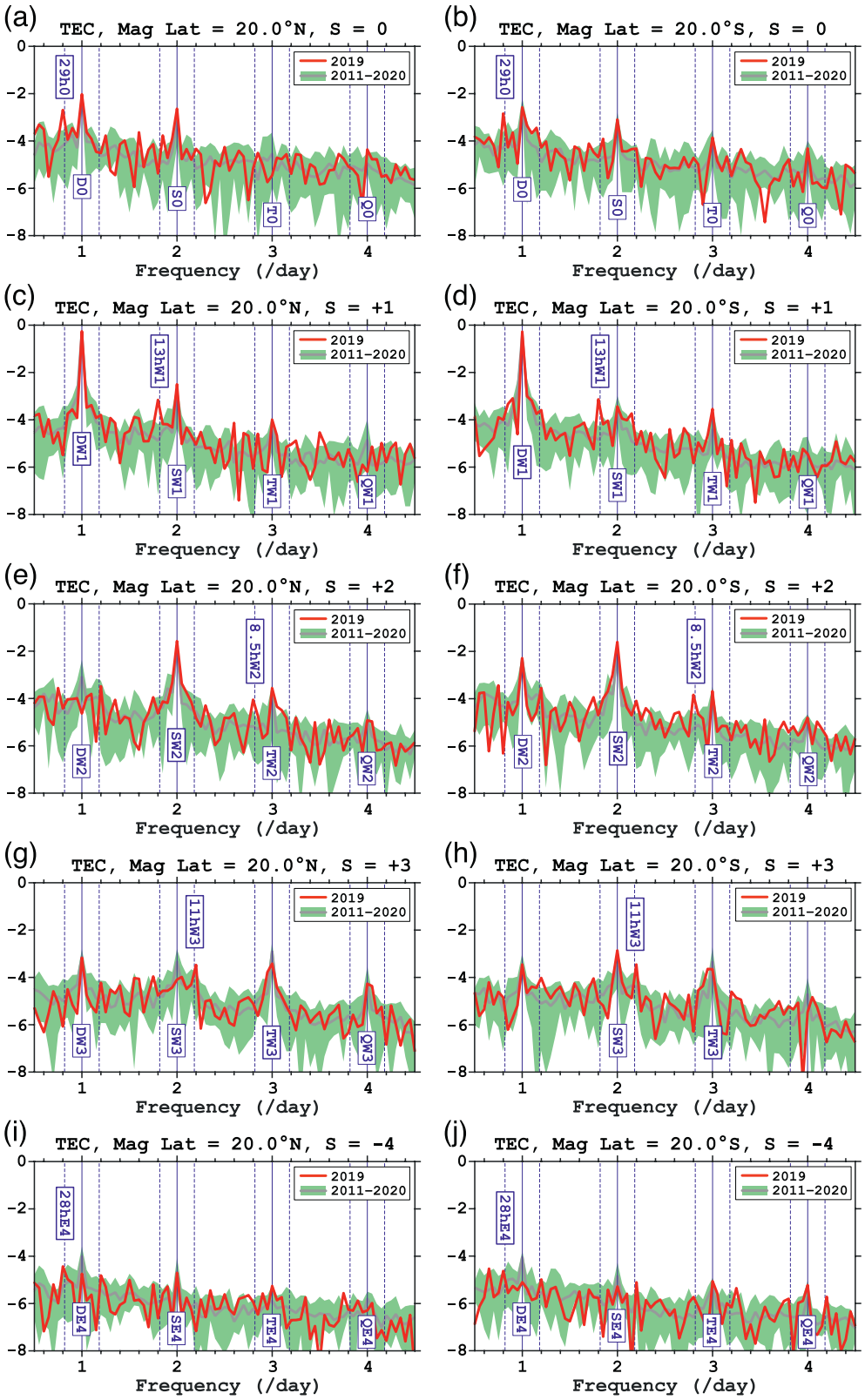
(a)
TEC, Mag Lat = 20.0°N, S = 0
29h0
D0
S0
T0
Q0
(b)
TEC, Mag Lat = 20.0°S, S = 0
29h0
D0
S0
T0
Q0
(c)
TEC, Mag Lat = 20.0°N, S = +1
13hW1
DW1
SW1
TW1
QW1
(d)
TEC, Mag Lat = 20.0°S, S = +1
13hW1
DW1
SW1
TW1
QW1
(e)
TEC, Mag Lat = 20.0°N, S = +2
8.5hW2
DW2
SW2
TW2
QW2
(f)
TEC, Mag Lat = 20.0°S, S = +2
8.5hW2
DW2
SW2
TW2
QW2
(g)
TEC, Mag Lat = 20.0°N, S = +3
11hW3
DW3
SW3
TW3
QW3
(h)
TEC, Mag Lat = 20.0°S, S = +3
11hW3
DW3
SW3
TW3
QW3
(i)
TEC, Mag Lat = 20.0°N, S = -4
28hE4
DE4
SE4
TE4
QE4
(j)
TEC, Mag Lat = 20.0°S, S = -4
28hE4
DE4
SE4
TE4
QE4
2019
2011–2020
Frequency (/day)

with other years' because the relative amplitude of ionospheric variability tends to be independent of solar activity (e.g., Wang et al., 2015; Yamazaki, 2018). The vertical solid lines correspond to tides, while the vertical dashed lines correspond to secondary waves from the Q6DW-tidal interaction.

Strong signatures of 29h0 are seen in Figures 2a and 2b, which can be attributed to the non-linear interaction of the Q6DW and DW1. Similarly, 13hW1 signatures are seen in Figures 2c and 2d, which are attributable to the Q6DW-SW2 interaction. 11hW3 signatures seen in Figures 2g and 2h can also be attributed to the Q6DW-SW2 interaction. 8.5hW2 signatures in Figures 2e and 2f can arise from the Q6DW-TW3 interaction. Signatures of 7.5hW4, which are also attributable to the Q6DW-TW3 interaction, are found in the results for $s = +4$ (not shown here). These signatures are all well separated from the climatological mean over the years 2011–2018 and 2020 by more than three times the standard deviation, and thus significant at >99% confidence levels. The only exception is the signatures of 11hW3 at 20°N magnetic latitude, which is significant at the 95% confidence level. The results suggest that the non-linear interaction between the Q6DW and various migrating tides occurred during the Q6DW event in September 2019. It is noted that spectral peaks corresponding to 21hW2 are also visible in Figures 2e and 2f, but they are not much larger than those observed during other years.

Evidence is also found for the non-linear interaction between the Q6DW and non-migrating tides. For example, 28hE4 signatures in Figures 2i and 2j, detected at the 95% and 90% confidence levels, respectively, can be attributed to the Q6DW-DE3 interaction. Spectral peaks related to 21hE2 are also found in the results for $s = -2$ (not shown here), but signatures are not much larger than other years'. We note that secondary wave signatures associated with the Q6DW interaction with non-migrating tides are not as prominent as those associated with the Q6DW interaction with migrating tides.

The amplitudes and phases of 29h0, 13hW1, 11hW3, 8.5hW2, and 29hE4 signatures in TEC are presented in Figure 3. In all cases, amplitude maxima can be found at ±20° magnetic latitudes, reflecting the latitudinal structure of the equatorial ionization anomaly. The latitudinal structures of the phases are largely symmetric about the magnetic equator. These results suggest that the secondary-wave signatures in the ionosphere are produced by the modulation of the equatorial electric field and the accompanying modulation of the equatorial ionization anomaly. The wave signatures are largest on 21–22 September 2019, roughly corresponding to the time when the Q6DW in the middle atmosphere was strongest (Figure 1c). The maximum amplitudes of the signatures are 8.0% for 29h0, 5.5% for 13hW1, 4.2% for 11hW3, 2.7% for 8.5hW2, and 1.4% for 29hE4. The secondary-wave signatures are also enhanced around August 30, 2019, which also corresponds to a minor burst of the Q6DW (Figure 1c). These results indicate the link between Q6DW activity in the middle atmosphere and excitation of the secondary waves.

3.3. GAIA Results

Figures 4a–4d present Fourier spectra of TEC for the zonal wavenumber $s = 0$ and $s = +1$ in a similar format as Figures 2a–2d. In each panel, the results are compared between the observations (red) and GAIA predictions (black). Although the data-model agreement is by no means perfect, GAIA is able to reproduce spectral peaks associated with secondary waves from the non-linear interaction between the Q6DW and tides. For example, the signatures of 29h0 are seen in Figures 4a and 4b, and those of 13hW1 are seen in Figures 4c and 4d. Similarly, GAIA results showed peaks at 11hW3, 8.5hW2, and 28hE4 (not shown here).

Figures 4e, 4g, and 4i show the relative amplitude of 29h0, 13hW1, and 11hW3 in TEC derived from GAIA; see also Figures 3a, 3c, and 3e for comparison. GAIA reproduces salient features of these wave signatures in TEC including the latitudinal structure and temporal variation. Figures 4f, 4h, and 4j are the same as Figures 4e, 4g, and 4i but modified wind forcing is used to drive the ionospheric model of GAIA. The simulation with modified wind forcing was performed only around September 20, 2019 when the secondary

Figure 2. Frequency versus amplitude spectrum of total electron content (TEC) from global ionospheric maps at 20°N (a, c, e, g, and i) and 20°S (b, d, f, h, and j) magnetic latitudes for the zonal wavenumber $s = 0$ (a and b), $s = +1$ (c and d), $s = +2$ (e and f), $s = +3$ (g and h), and $s = -4$ (g and h) during 10–30 September 2019. The vertical axis represents the logarithm of the amplitude (in %) relative to the zonal mean TEC. The red lines show the results for 2019. The green shading indicates the maximum and minimum values observed during other years (2011–2018 and 2020) and the gray lines show average spectra over those years. The frequencies of tides and secondary waves due to the non-linear interaction between the quasi-6-day wave and tides are indicated.

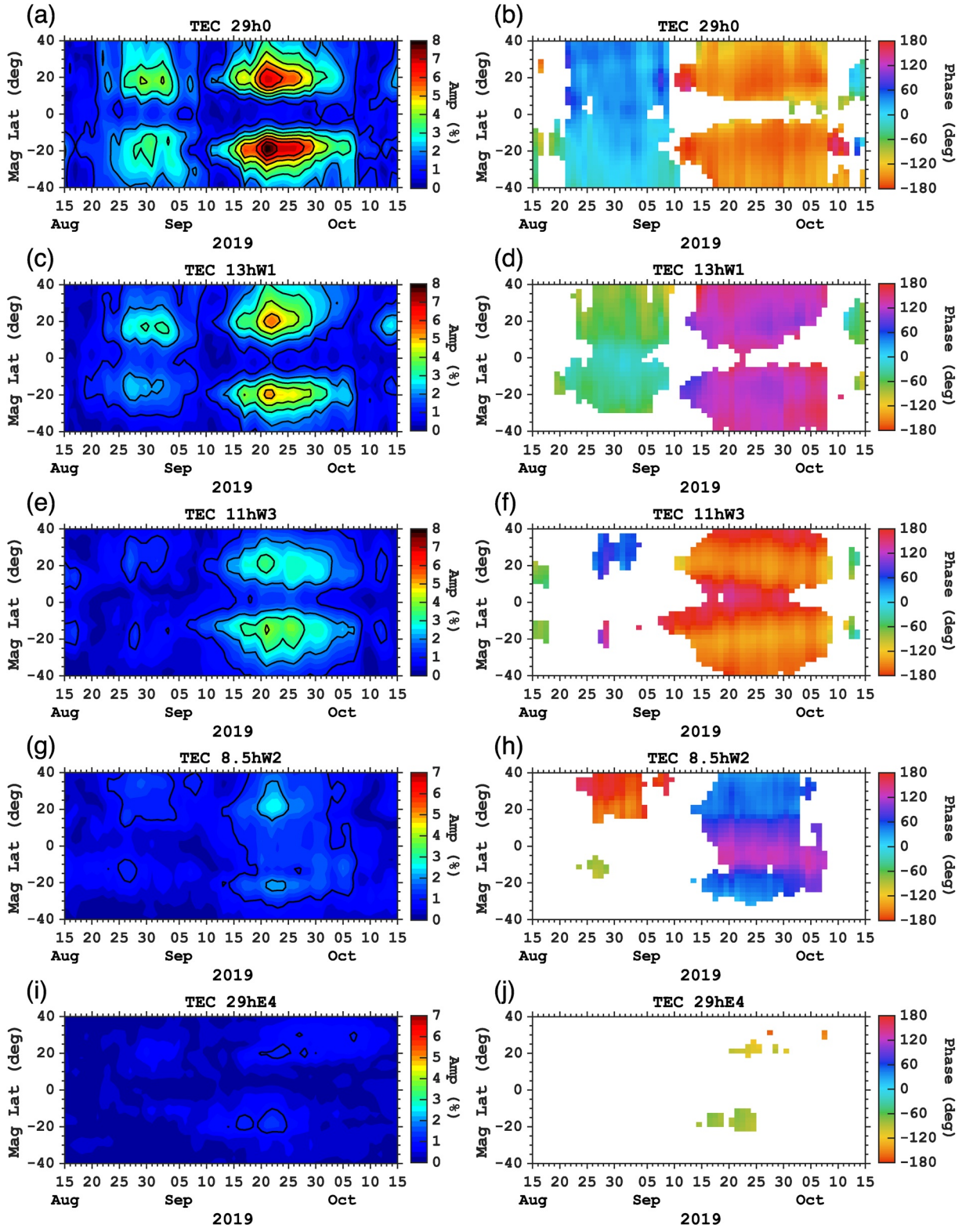

Figure 3. The relative amplitude (a, c, e, g, and i) and phase (b, d, f, h, and j) of wave signatures in total electron content (TEC) during 15 August to October 15, 2019: (a and b) 29h0 from the Q6DW interaction with DW1, (c and d) 13hW1 from the Q6DW interaction with SW2, (e and f) 11hW3 from the Q6DW interaction with SW2, (g and h) 8.5hW2 from the Q6DW interaction with TW3, and (i and j) 29hE4 from the Q6DW interaction with DE3. The phase is shown only where the relative amplitude is greater than 1% of the zonal mean TEC. TEC, total electron content.

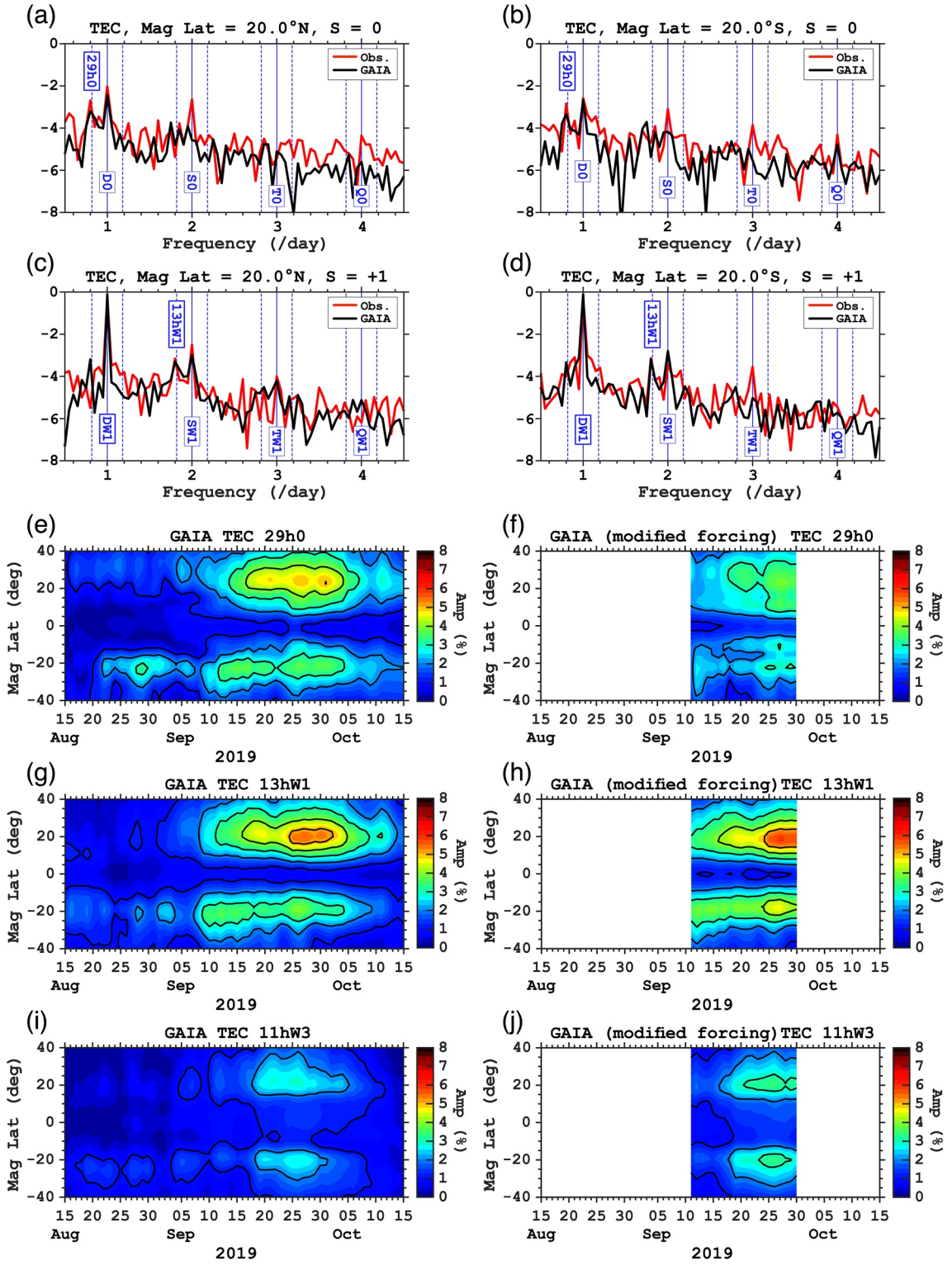

Figure 4. (a–d) are the same as Figures 2a–2d except for the GAIA simulation results (black) along with the corresponding observations (red). (e, g, and i) are the same as Figures 3a, 3c, and 3e except for the GAIA simulation results. (f, h, and j) are the same as (e, g, and i) except for the simulation results with modified wind forcing that excludes waves with periods longer than 36 h. See text in Section 2 for more details on the modified forcing. GAIA, Ground-to-topside model of Atmosphere and Ionosphere for Aeronomy.

wave signatures are most prominent. As explained in Section 2, modified wind forcing excludes waves with periods longer than 36 h (e.g., Q6DW) while it retains tides and secondary waves from the tidal interaction with long-period waves (e.g., 29h0, 13hW1, and 11hW3). The results from the simulation with modified wind forcing are largely in agreement with the original GAIA results. This suggests that 29h0, 13hW1, and 11hW3 signatures in TEC are due in large part to forcing by the secondary waves in the neutral atmosphere. The slight difference between the two results, which is most evident for 29h0 (up to 1.5%), suggests that waves with periods longer than 36 h can also contribute to secondary-wave signatures in TEC. A possible explanation is the interaction between the Q6DW and diurnally varying ionosphere. The low- and middle-latitude ionosphere undergoes a diurnal cycle due to enhanced ionization on the dayside, which introduces DW1 signatures in ionospheric parameters (e.g., Chang et al., 2013). Thus, the interaction between neutral parameters with Q6DW signatures and ionospheric parameters with DW1 signatures can lead to 29h0 signatures.

4. Summary and Conclusions

The present study examined ionospheric signatures of short-period (5–48 h) waves during the September 2019 Antarctic SSW, which was accompanied by an exceptionally strong Q6DW in the MLT region (Figure 1). A Fourier analysis was performed on global total electron content (TEC) maps to derive spectra for different zonal wavenumbers (Figure 2). It is found that signatures of 29h0, 13hW1, 11hW3, 8.5hW2, and 28hE4 in TEC at low latitudes are strong compared to those observed during the same time of other years (2011–2018 and 2020). These signatures are attributed to the secondary waves from the non-linear interaction between the Q6DW and atmospheric tides.

Ionospheric signatures of 29h0, 13hW1, 11hW3, 8.5hW2, and 28hE4 are symmetric with respect to the magnetic equator with amplitude maxima at ±20° magnetic latitudes (Figure 3), indicating that they are driven through the modulation of the equatorial plasma fountain. The secondary wave signatures are largest around maximum Q6DW activity in the middle atmosphere. The maximum amplitudes of the wave signatures in TEC are 8.0%, 5.5%, 4.2%, 2.7%, and 1.4% of the zonal mean TEC for 29h0, 13hW1, 11hW3, 8.5hW2, and 29hE4, respectively.

GAIA is able to reproduce spectral peaks in TEC at low latitudes related to the Q6DW-tidal interaction (Figure 4). Our simulation using high-pass filtered winds indicates that the main energy of the 13hW1 and 11hW3 signatures in TEC and part energy of the 29h0 signature are contributed by the modulations of the plasma fountain by the corresponding secondary waves in the neutral atmosphere. The direct modulation of the plasma fountain by the Q6DW contributes significantly only to the 29h0 TEC signature.

The results presented in this study, along with those in the accompanying paper MY20, provide compelling evidence to support ionospheric wind dynamo effects of the secondary waves due to the non-linear interaction between the Q6DW and tides during the September 2019 Antarctic SSW.

Data Availability Statement

The global TEC maps used in this paper were provided by Universitat Politécnica de Catalunya (UPC) and downloadable from the SPDF CDAWeb database (https://cdaweb.gsfc.nasa.gov/index.html/). The simulation data used in this study are available from GFZ Data Services (https://doi.org/10.5880/GFZ.2.3.2020.004). The geomagnetic activity index *Ap* was provided by the GFZ German Research Center for Geosciences (https://www.gfz-potsdam.de/en/kp-index/). The solar activity index $F_{10.7}$ was downloaded from the SPDF OMNIWeb database (https://omniweb.gsfc.nasa.gov).

Acknowledgments
We thank the NASA Goddard Earth Sciences (GES) Data and Information Services Center (DISC) (https://disc.gsfc.nasa.gov/) for making the Aura/MLS GPH data (https://doi.org/10.5067/Aura/MLS/DATA2008) and MERRA-2 data (DOI: 10.5067/QBZ6MG944HW0) available. This work was supported in part by ESA through contract 4000126709/19/NL/IS "VERA" and by JSPS and DFG (grant YA-574-3-1) under the Joint Research Projects-LEAD with DFG (JRPs-LEAD with DFG). Open access funding enabled and organized by Projekt DEAL.

References

Beard, A. G., Mitchell, N. J., Williams, P. J. S., & Kunitake, M. (1999). Non-linear interactions between tides and planetary waves resulting in periodic tidal variability. *Journal of Atmospheric and Solar-Terrestrial Physics*, *61*(5), 363–376. https://doi.org/10.1016/s1364-6826(99)00003-6

Chang, L. C., Lin, C.-H., Liu, J.-Y., Balan, N., Yue, J., & Lin, J.-T. (2013). Seasonal and local time variation of ionospheric migrating tides in 2007-2011 FORMOSAT-3/COSMIC and TIE-GCM total electron content. *Journal of Geophysical Research: Space Physics*, *118*(5), 2545–2564. https://doi.org/10.1002/jgra.50268

Chau, J., Goncharenko, L. P., Fejer, B. G., & Liu, H.-L. (2012). Equatorial and low latitude ionospheric effects during sudden stratospheric warming events. *Space Science Reviews*, *168*(1–4), 385–417. https://doi.org/10.1007/s11214-011-9797-5

Emmert, J., Richmond, A., & Drob, D. (2010). A computationally compact representation of magnetic-apex and quasi-dipole coordinates with smooth base vectors. *Journal of Geophysical Research*, *115*(A8). https://doi.org/10.1029/2010ja015326

Forbes, J. M., & Zhang, X. (2017). The quasi-6 day wave and its interactions with solar tides. *Journal of Geophysical Research: Space Physics*, *122*(4), 4764–4776. https://doi.org/10.1002/2017ja023954

Forbes, J. M., Zhang, X., Palo, S., Russell, J., Mertens, C., & Mlynczak, M. (2008). Tidal variability in the ionospheric dynamo region. *Journal of Geophysical Research*, *113*(A2). https://doi.org/10.1029/2007ja012737

Gan, Q., Oberheide, J., Yue, J., & Wang, W. (2017). Short-term variability in the ionosphere due to the nonlinear interaction between the 6 day wave and migrating tides. *Journal of Geophysical Research: Space Physics*, *122*(8), 8831–8846. https://doi.org/10.1002/2017ja023947

Gelaro, R., McCarty, W., Suárez, M. J., Todling, R., Molod, A., Takacs, L., et al. (2017). The modern-era retrospective analysis for research and applications, version 2 (MERRA-2). *Journal of Climate*, *30*(14), 5419–5454. https://doi.org/10.1175/jcli-d-16-0758.1

Goncharenko, L. P., Chau, J. L., Condor, P., Coster, A., & Benkevitch, L. (2013). Ionospheric effects of sudden stratospheric warming during moderate-to-high solar activity: Case study of January 2013. *Geophysical Research Letters*, *40*(19), 4982–4986. https://doi.org/10.1002/grl.50980

Goncharenko, L. P., Coster, A., Chau, J., & Valladares, C. (2010). Impact of sudden stratospheric warmings on equatorial ionization anomaly. *Journal of Geophysical Research*, *115*(A10). https://doi.org/10.1029/2010ja015400

Hayashi, Y. (1971). A generalized method of resolving disturbances into progressive and retrogressive waves by space Fourier and time cross-spectral analyses. *Journal of the Meteorological Society of Japan*, *49*(2), 125–128. https://doi.org/10.2151/jmsj1965.49.2_125

Hernández-Pajares, M., Juan, J., Sanz, J., Orus, R., Garcia-Rigo, A., Feltens, J., et al. (2009). The IGS VTEC maps: A reliable source of ionospheric information since 1998. *Journal of Geodesy*, *83*(3–4), 263–275. https://doi.org/10.1007/s00190-008-0266-1

Jin, H., Miyoshi, Y., Fujiwara, H., & Shinagawa, H. (2008). Electrodynamics of the formation of ionospheric wave number 4 longitudinal structure. *Journal of Geophysical Research*, *113*(A9). https://doi.org/10.1029/2008ja013301

Jin, H., Miyoshi, Y., Fujiwara, H., Shinagawa, H., Terada, K., Terada, N., et al. (2011). Vertical connection from the tropospheric activities to the ionospheric longitudinal structure simulated by a new earth's whole atmosphere-ionosphere coupled model. *Journal of Geophysical Research*, *116*(A1). https://doi.org/10.1029/2010ja015925

Jin, H., Miyoshi, Y., Pancheva, D., Mukhtarov, P., Fujiwara, H., & Shinagawa, H. (2012). Response of migrating tides to the stratospheric sudden warming in 2009 and their effects on the ionosphere studied by a whole atmosphere-ionosphere model GAIA with COSMIC and TIMED/SABER observations. *Journal of Geophysical Research*, *117*(A10). https://doi.org/10.1029/2012ja017650

Kobayashi, S., Ota, Y., Harada, Y., Ebita, A., Moriya, M., Onoda, H., et al. (2015). The JRA-55 reanalysis: General specifications and basic characteristics. *Journal of the Meteorological Society of Japan*, *93*(1), 5–48. https://doi.org/10.2151/jmsj.2015-001

Krüger, K., Naujokat, B., & Labitzke, K. (2005). The unusual midwinter warming in the southern hemisphere stratosphere 2002: A comparison to northern hemisphere phenomena. *Journal of the Atmospheric Sciences*, *62*(3), 603–613. https://doi.org/10.1175/jas-3316.1

Lin, J.-T., Lin, C.-H., Rajesh, P., Yue, J., Lin, C., & Matsuo, T. (2020). Local-time and vertical characteristics of quasi-6-day oscillation in the ionosphere during the 2019 antarctic sudden stratospheric warming. *Geophysical Research Letters*, *47*(21), e2020GL090345. https://doi.org/10.1029/2020gl090345

Lindzen, R. S., & Chapman, S. (1969). Atmospheric tides. *Space Science Reviews*, *10*(1), 3–188. https://doi.org/10.1007/bf00171584

Liu, H.-L. (2016). Variability and predictability of the space environment as related to lower atmosphere forcing. *Space Weather*, *14*(9), 634–658. https://doi.org/10.1002/2016sw001450

Miyoshi, Y., & Fujiwara, H. (2003). Day-to-day variations of migrating diurnal tide simulated by a GCM from the ground surface to the exobase. *Geophysical Research Letters*, *30*(15). https://doi.org/10.1029/2003gl017695

Miyoshi, Y., Fujiwara, H., Jin, H., Shinagawa, H., Liu, H., & Terada, K. (2011). Model study on the formation of the equatorial mass density anomaly in the thermosphere. *Journal of Geophysical Research*, *116*(A5). https://doi.org/10.1029/2010ja016315

Miyoshi, Y., Pancheva, D., Mukhtarov, P., Jin, H., Fujiwara, H., & Shinagawa, H. (2017). Excitation mechanism of non-migrating tides. *Journal of Atmospheric and Solar-Terrestrial Physics*, *156*, 24–36. https://doi.org/10.1016/j.jastp.2017.02.012

Miyoshi, Y., & Yamazaki, Y. (2020). Excitation mechanism of ionospheric 6-day oscillation during the 2019 september sudden stratospheric warming event. *Journal of Geophysical Research: Space Physics*, *125*(9), e2020JA028283. https://doi.org/10.1029/2020ja028283

Oberheide, J., Pedatella, N., Gan, Q., Kumari, K., Burns, A., & Eastes, R. (2020). Thermospheric composition O/N_2 response to an altered meridional mean circulation during sudden stratospheric warmings observed by gold. *Geophysical Research Letters*, *47*(1), e2019GL086313. https://doi.org/10.1029/2019gl086313

Olson, M. E., Fejer, B. G., Stolle, C., Lühr, H., & Chau, J. L. (2013). Equatorial ionospheric electrodynamic perturbations during southern hemisphere stratospheric warming events. *Journal of Geophysical Research: Space Physics*, *118*(3), 1190–1195. https://doi.org/10.1002/jgra.50142

Orús, R., Hernández-Pajares, M., Juan, J. M., & Sanz, J. (2005). Improvement of global ionospheric VTEC maps by using kriging interpolation technique. *Journal of Atmospheric and Solar-Terrestrial Physics*, *67*(16), 1598–1609. https://doi.org/10.1016/j.jastp.2005.07.017

Pancheva, D., Haldoupis, C., Meek, C., Manson, A., & Mitchell, N. (2003). Evidence of a role for modulated atmospheric tides in the dependence of sporadic e layers on planetary waves. *Journal of Geophysical Research*, *108*(A5). https://doi.org/10.1029/2002ja009788

Pancheva, D., Miyoshi, Y., Mukhtarov, P., Jin, H., Shinagawa, H., & Fujiwara, H. (2012). Global response of the ionosphere to atmospheric tides forced from below: Comparison between cosmic measurements and simulations by atmosphere-ionosphere coupled model gaia. *Journal of Geophysical Research*, *117*(A7). https://doi.org/10.1029/2011ja017452

Pedatella, N., Chau, J., Schmidt, H., Goncharenko, L., Stolle, C., Hocke, K., et al. (2018). How sudden stratospheric warming affects the whole atmosphere. *Eos*, *99*, 35–38. https://doi.org/10.1029/2018eo092441

Pedatella, N., Liu, H.-L., & Hagan, M. (2012). Day-to-day migrating and nonmigrating tidal variability due to the six-day planetary wave. *Journal of Geophysical Research*, *117*(A6). https://doi.org/10.1029/2012ja017581

Riggin, D. M., Liu, H.-L., Lieberman, R. S., Roble, R. G., Russell, J. M., III, Mertens, C. J., et al. (2006). Observations of the 5-day wave in the mesosphere and lower thermosphere. *Journal of Atmospheric and Solar-Terrestrial Physics*, *68*(3–5), 323–339. https://doi.org/10.1016/j.jastp.2005.05.010

Roma-Dollase, D., Hernández-Pajares, M., Krankowski, A., Kotulak, K., Ghoddousi-Fard, R., Yuan, Y., et al. (2018). Consistency of seven different GNSS global ionospheric mapping techniques during one solar cycle. *Journal of Geodesy*, *92*(6), 691–706. https://doi.org/10.1007/s00190-017-1088-9

Schwartz, M., Lambert, A., Manney, G., Read, W., Livesey, N., Froidevaux, L., et al. (2008). Validation of the aura microwave limb sounder temperature and geopotential height measurements. *Journal of Geophysical Research*, *113*(D15). https://doi.org/10.1029/2007JD008783

Shinagawa, H. (2011). Ionosphere simulation. *Journal of NICT*, *56*(1–4), 199–207.
Tapping, K. F. (2013). The 10.7 cm solar radio flux ($F_{10.7}$). *Space Weather*, *11*(7), 394–406. https://doi.org/10.1002/swe.20064
Teitelbaum, H., & Vial, F. (1991). On tidal variability induced by nonlinear interaction with planetary waves. *Journal of Geophysical Research*, *96*(A8), 14169–14178. https://doi.org/10.1029/91ja01019
Wang, S., Huang, S., & Fang, H. (2015). Wave-3 and wave-4 patterns in the low- and mid-latitude ionospheric TEC. *Journal of Atmospheric and Solar-Terrestrial Physics*, *132*, 82–91. https://doi.org/10.1016/j.jastp.2015.07.002
Waters, J. W., Froidevaux, L., Harwood, R. S., Jarnot, R. F., Pickett, H. M., Read, W. G., et al. (2006). The earth observing system microwave limb sounder (eos mls) on the aura satellite. *IEEE Transactions on Geoscience and Remote Sensing*, *44*(5), 1075–1092.
Yamazaki, Y. (2018). Quasi-6-day wave effects on the equatorial ionization anomaly over a solar cycle. *Journal of Geophysical Research: Space Physics*, *123*(11), 9881–9892. https://doi.org/10.1029/2018ja026014
Yamazaki, Y., Matthias, V., Miyoshi, Y., Stolle, C., Siddiqui, T., Kervalishvili, G., et al. (2020). September 2019 Antarctic sudden stratospheric warming: Quasi-6-day wave burst and ionospheric effects. *Geophysical Research Letters*, *47*(1), e2019GL086577. https://doi.org/10.1029/2019gl086577
Yamazaki, Y., & Miyoshi, Y. (2020). *Simulation data from GAIA (Ground-to-Topside Model of Atmosphere and Ionosphere for Aeronomy) for the September 2019 Sudden Stratospheric Warming Event*. GFZ Data Services. https://doi.org/10.5880/GFZ.2.3.2020.004
Yamazaki, Y., Miyoshi, Y., Xiong, C., Stolle, C., Soares, G., & Yoshikawa, A. (2020). Whole atmosphere model simulations of ultrafast Kelvin wave effects in the ionosphere and thermosphere. *Journal of Geophysical Research: Space Physics*, *125*(7), e2020JA027939. https://doi.org/10.1029/2020JA027939